

Power deposition on the ergodic divertor in Tore Supra : review and prospects.

L. Costanzo, T. Loarer, Ph. Ghendrih, D. Guilhem,
J. P. Gunn, P. Monier-Garbet, B. Pégourié, P. Thomas

*Association Euratom-CEA sur la Fusion contrôlée, CEA Cadarache,
13108 Saint Paul Lez Durance, France*

1. Introduction

Handling the high energy flux deposited on the inner wall is an important issue for the scaling of future fusion devices. In diverted tokamak, a considerable part of the outgoing power is channelled on the target plates via the parallel heat flux (Q_{\parallel}). Measurement and control of Q_{\parallel} is therefore a crucial point to allow the divertor and consequently the reactor to survive such power density. Over the past years, the Tore Supra ergodic divertor has demonstrated capabilities to control particle and heat fluxes in the plasma edge. This paper reports on a wide range of ergodic divertor results concerning the power deposition on the target plates. One of the primary purpose is to evaluate the dependence of the heat flux according to various experimental conditions. Section 2 describes in the broad outline the characteristics of the ergodic divertor. In section 3, the effect of the magnetic perturbation on heat flux is considered. Experimental evidences of low heat flux values in ergodic divertor configuration are presented. In this section, we discuss the influence of the working gas on the power deposition. Toroidal profiles along the wetted area of the neutraliser plate when additional heating is applied are reported. Section 4 is dedicated to the sheath heat transmission factor, parameter directly proportional to the heat flux and which is crucial in the absolute value of Q_{\parallel} . Detachment is a key parameter and section 5 is devoted to a new infrared degree of detachment. Section 6 addresses the issue of the power deposition in the new generation ergodic divertor. Finally, in section 7, we present the conclusions.

2. The ergodic divertor

In the ergodic divertor configuration, the magnetic surfaces are destroyed in the edge plasma with a resonant perturbation, leading to an edge layer where the field lines are stochastic [Ghe 96]. The magnetic perturbation is created by six modular coils equally spaced toroidally inside the vacuum vessel. A view of one module is given in figure 1. The modules are equipped with actively cooled neutraliser plates implemented between the current bars and coated with boron carbide (B_4C). In the edge region, the magnetic deflection of the field lines to dedicated wall components generates specific patterns of power deposition [Ghe 97]. The ergodic divertor has demonstrated its capability to control energy and particle deposition, while providing both a significant screening of impurities and stable radiating layers [DeM 95]. It allows an increase of the total radiated power at the edge while minimizing the plasma contamination via edge screening of impurity influxes (preventing the impurity species to reach the plasma bulk). The ergodic divertor offers the possibility to obtain a cool and dense plasma at the edge allowing a low power deposition. Moreover, the physical sputtering is strongly reduced and the pumping efficiency is rather good [Gro 92].

The heat flux flowing to the divertor target plates can be determined by two different diagnostics. Fourteen Langmuir probes (LP) are installed on the neutraliser plates at different poloidal and toroidal locations. Figure 2 shows a neutraliser plate equipped with four probes (three can be seen on the picture) embedded between the actively cooled fingers. Thermographic measurements viewing these neutraliser plates are performed simultaneously using three high resolution infrared cameras located at 120° toroidal sectors. An example of the thermal image of a neutraliser plate is given in figure 3. The view illustrates an experimental surface temperature map which can be directly interpreted in terms of power

density. One can clearly see a non uniform power deposition corresponding to different flux tubes and hot spots corresponding to the Langmuir probes which are not actively cooled.

3. Heat flux parametric study

All the reported experiments have been performed with the standard resonant ergodic divertor configuration : toroidal field $B_T = 3,1$ T, plasma current $I_p = 1,4$ MA, major radius $R = 2,39$ m and edge safety factor $q_\psi = 3$. The figure 4 shows the variation of power deposition along a neutraliser as a function of the divertor current (I_{ED}) which determines the magnitude of the divertor perturbation. Heat flux on the neutraliser grows in a quasi linear way with the perturbation. This increase is accompanied by a reduction of power deposition on the outboard pumped limiter (OPL). One also notices that the energy flux is peaked, corresponding to an intrinsic property of the ergodic divertor. The peaking factor grows with the divertor current [Gro 97].

Concerning the effect of the conducted power P_{Cond} (= Total Power P_{Tot} - Radiated power P_{Rad}) on the power deposition in ergodic divertor configuration, several points should be underlined. Figure 5 highlights the low values of energy flux striking the neutralisers in spite of very high levels of injected power in comparison with a limiter discharge. For 2 MW of conducted power, the parallel heat flux on the limiter is ~ 17 MW/m² whereas it is "only" ~ 2.5 MW/m² for the divertor case. A change of regime takes place around $P_{Cond} \sim 5$ MW with a strong increase of the heat flux beyond this value. However the lack of experimental data beyond 6 MW (the majority of the shots has been performed with P_{Cond} below 6MW) makes difficult the confirmation of this tendency.

Edge plasma parameters are modified both by injecting extrinsic impurity like neon and by using Ion Cyclotron Resonance Heating (ICRH). Density scans are systematically considered for the reported experiments. The heat flux is here measured by Langmuir probes. Figure 6

illustrates the role of power balance in the density limit. Injection of neon into the discharge results in increased radiated power and lower heat flux for the same density. The limit density is lower but occurs at roughly the same value of heat flux, in this case $\sim 0.5 \text{ MW/m}^2$. Other studies have shown that detachment occurs earlier when neon is injected [Gun 99]. Figure 7 gives the evolution of $Q_{||}$ versus the volume averaged density ($\langle n_e \rangle$) for deuterium discharges. A clear shift to high averaged plasma volume density with increasing power level is observed. When the input power rises, the operating density is higher. The strong oscillations of the parallel heat flux are linked to the sawteeth which occur at high ICRH heating.

The global tendency is : all that provides power shifts towards the high densities and all that consumes power (like radiation) shifts towards the low densities.

The evolution of heat flux during the application of the additional power is a determining element in the comparison of the two studied gases. Figure 8 represents the evolution of the mean parallel heat flux (averaged value during the ICRH pulse) as a function of the total input power. An increase is observed for both gases but it is much higher in helium than in deuterium. For deuterium discharges, the curve highlights values varying from 3 MW/m^2 for 1.5 MW of injected power to 9 MW/m^2 for $P_{\text{Tot}} = 5 \text{ MW}$. This tendency is confirmed for successive discharges or not, excluding a problem of wall content historic. Moreover, the behaviour is similar in the case of measurements resulting from different divertor module confirming a toroidal symmetry. In helium case, the values vary between 6 and 20 MW/m^2 for an injected power from 2 to 5.5 MW . This different behaviour can be attributed to a better particle screening effect in deuterium which is one of the most important effects which results from the ergodic divertor use. This is due to the longer mean free path for helium and the different charge exchange cross section. The neutral density is different and should be taken into account. Indeed, the recycling flux, the wall particle content and the resulting outgasing

are much higher in deuterium which very likely leads to a larger neutral density at the edge. Also, the radiated power is greater in deuterium than in helium and this supports this idea.

A significant point concerning the effect of the power is the standardization of the energy deposition at strong power level. One can note it on the evolution of the heat flux profile along a neutraliser finger for various power levels (figure 9). The profile is peaked at low power level and it becomes almost flat at 4 MW. The increase in perpendicular transport with the application of additional power is the cause of this standardization.

4. Sheath heat transmission factor

The sheath heat transmission factor γ is used to calculate the parallel heat flux obtained with the Langmuir probes. The standard sheath theory yields $\gamma = 7$ for deuterium plasma with ion temperature equal to electron temperature [Pit 97]. It plays an important role in terms of thermal exchange between ions and electrons in the sheath. In Tore Supra, the correlation between the heat flux deduced from Langmuir probes and infrared measurements allows one to determine an experimental value of this factor :

$$\gamma_{\text{exp}} = \frac{Q_{//\text{IR}}}{\Gamma_{//} T_{\text{e_edge}}} \quad (1)$$

where $Q_{//\text{IR}}$ is the parallel heat flux deduced from the infrared measurements, $T_{\text{e_edge}}$ the electron temperature and $\Gamma_{//}$ the parallel particle flux.

As illustrated on figure 10, a typical increase of γ_{exp} from ~ 7.5 to $\sim 10-11$ respectively for $P_{\text{tot}} \sim 1$ to 5 MW is observed with the total input power independently of the working gas. Such high values of γ_{exp} for auxiliary heated discharges can be interpreted by a T_i / T_e ratio around 2-3. The increase in the size of the error bars at high input power is due to the sawtooth crashes. Nevertheless, some ohmic shots in “pure“ helium are significantly lower than the normally accepted $\gamma = 7$ value. The involved evolution is shown on figure 11 where γ_{exp} is

plotted as a function of the edge electronic temperature T_{e_edge} for one characteristic shot in “pure” D₂ and one shot in “pure” He. While for D₂ γ_{exp} remains close to 7 over the all T_{e_edge} range, for He, the γ_{exp} becomes as low as 2 or 3 for low edge temperature, (i.e. $T_{e_edge} \sim 10$ eV). From $T_{e_edge} \sim 15$ eV to ~ 30 eV, a linear increase of γ_{exp} is observed while for higher temperature, $T_{e_edge} \sim 30 - 50$ eV ($\langle n_e \rangle \sim 4 \cdot 10^{19} \text{ m}^{-3}$), the standard value of $\gamma \sim 7$ is recovered [Cos 01a]. Neither the theoretical point of view nor the simulations done with the exploitation of the one-dimensional particle-in-cell code called " Plasma Device Planar 1 Dimension " (PDP1) [Bir 91, Ver 93, Ver 95] have led to values as low as experimentally obtained. The assumption that seems to be the most probable to explain these low values is an overestimation of the electron temperature given by the Langmuir probes under certain conditions. Langmuir probes measurements are based on the assumption of a Maxwellian electron distribution. An energetic electron tail can affect the value of the sheath potential. The non-Maxwellian tail can significantly affect plasma diagnostics, parallel heat fluxes, plasma-neutral and plasma-impurities interactions. This tail of electrons can result in an overestimate of the temperature by probes by at least a factor 2 [Bat 97]. However, the absence of appropriate diagnosis in the edge plasma to determine the presence or the absence of this population does not allow to conclude in an absolute way. However, a major element emerges from this study : in the majority of the cases, it is experimentally and numerically confirmed that $\gamma = 7$. This value is valid for ohmic discharges with deuterium injection and most of the time in helium.

If γ is now assumed to be correct, it is possible to calculate an infrared edge electronic temperature as follow :

$$T_{e_edge} \text{ " IR " } = \frac{Q_{//IR}}{7\Gamma_{//}} \quad (2)$$

with the hypothesis that particle flux given by the probes is correct.

The figure 12 illustrates the comparison between the two temperatures for the helium case. A good agreement between the "Langmuir probe" temperature and the "Infrared" temperature is obtained at low plasma density. When the plasma density increases, the "IR" temperature is lower than the "LP" temperature. A value of 5 eV is obtained with infrared in helium. Such temperature has never been measured by the probes in Tore Supra. Moreover, it should be noted that the agreement between the temperatures is good at low density for the two gases, and then degrades oneself at high density in helium (with values not obtained in deuterium). This assumption implies that the temperature given by the probes is overestimated at high density.

5. 2D Infrared degree of detachment

By creating a dense and cold plasma in the neighbourhood of the divertor plates, it is possible to reach the "detached" regime, characterized by low electron temperature, strong reduction of particle flux and power flux on the plates, pressure drop along the field lines and significant fraction of radiated power in the SOL [Kra 95]. The non uniform power deposition patterns in the various configurations of divertor can involve difficulties to determine the Degree of Detachment (DoD) in particular with the fixed Langmuir probes. Infrared thermography measurements can be either local or integrated depending on the plasma configuration. We have developed a new way to measure detachment onset based on the parallel heat flux variation on the plates derived from the infrared signals. The analysis of experimental data during ergodic divertor operation on Tore Supra shows that the detachment occurs when the heat flux reaches a threshold value $Q_{//\text{Threshold}}$ which depends on the main plasma parameters (injected power, P_{Rad} , gas, $\langle n_e \rangle \dots$) and particularly on T_{e_edge} at the target plate. Figure 13 shows the evolution of $Q_{//}$ derived from infrared thermography versus T_{e_edge} for a density ramp up which detaches. A regular decrease of $Q_{//}$ is followed by a clear drop at $T_{e_edge} \sim 12$

eV, emphasizing the thermal flux sensitivity in the detachment phase. A similar behaviour between $Q_{//}$ and T_{e_edge} in terms of critical control parameter for detachment is highlighted [Cos 01b]. As soon as the plasma detaches, a sudden decrease of $Q_{//}$ is observed from 1.75 to 0.5 MW/m² respectively for $T_{e_edge} \sim 12$ eV and 10 eV. The notion of "infrared" DoD, based on the same concept as for the "probe" DoD, is proposed. It is defined as the ratio of the extrapolated heat flux in the high recycling regime ($Q_{//}^{adjusted}$) to the measured heat flux ($Q_{//}^{measured}$) as follows :

$$"IR" DoD = \frac{Q_{//}^{adjusted}}{Q_{//}^{measured}} . \quad (3)$$

This extrapolation is plotted on figure 13. The theory can lead to a calculated $Q_{//}^{adjusted}$ but the classical two point model doesn't fit very well with the ergodic divertor case and it is more effective to define an experimental value. Figure 14 exhibits the evolutions of two detachment criteria : probe and infrared. A very good agreement is observed between the criteria both in the amplitude (dynamic) and in the temporal behaviour. The slight advance in the infrared DoD is due to the easier (and therefore optimal) choice of the exposed zone with the infrared diagnosis.

The application of this method is direct on all the devices equipped with infrared cameras. The thermal time constant of the B₄C target surface layer is about 20 ms, the infrared image being thus a direct image of the heat flux impinging onto it (integration time of the cameras is 20 ms). Also the time resolution can be adjusted from 20 μs (JET) to 20 ms (Tore Supra) allowing to cancel the strong perturbation induced by the edge localized modes (ELMs) [Gau 01]. Moreover, in a reactor environment, it may be unacceptable to install target plate Langmuir probes. Infrared imaging obviously has a fundamental role to play in divertor diagnosis and feedback control.

The infrared camera provides a full 2D view of the target plate, and thus offers the possibility to follow any movement of the strike point. This is a distinct advantage of infrared

thermography over the fixed target probes, that give local measurements. This benefit in term of spatial resolution, since it takes into account the surface distribution, has led to a layout of 2D DoD map in real time. The detachment on the neutraliser is progressive and does not occur exactly in the same area that the probe since it depends on the geometry of the plasma configuration. With a 2D IR DoD, this problem is overcome. Figure 15 gives the infrared representations of a neutraliser for a same discharge at three different times. As shown in these figures, it is possible to follow the evolution of both the attached and detached zones on the neutraliser simultaneously. Figure 15_a illustrates an attached plasma. On figure 15_b, the detachment threshold value is reached on the upper finger whereas the rest of the interest zone is still attached. Figure 15_c represents a completely detached plasma.

6. Prospects

The ergodic divertor of Tore Supra was an original concept. In spite of this relative insulation compared to other machines equipped with axisymmetric divertor, excellent results were obtained. A possible strategy to use ergodic divertor in future devices is thus considered.

Ergodic divertor allows a spreading of power by radiation, a good screening of all impurity sources and a good pumping of hydrogenic species. No ELMs have been identified during the ergodic divertor operation on Tore Supra. Nevertheless, ELM control can be obtained with this type of divertor [Gro 01].

Concerning the particle collection, two way to improve the efficiency are available : increase the part of the plasma outflux interaction with the plate vented structure and optimize the geometry of the slots [Aze 00]. The radiation efficiency can be optimized when the gas injection is located at the divertor target plate instead of the vessel bottom [Mon 01]. Studies to compare the effectiveness of the ergodic divertor vs. axisymmetric divertors have also been done [Tho 01]. It is however difficult to make a choice between the ergodic and axisymmetric

divertor configurations. Each one has advantages and drawbacks. However, ergodic divertor has an undeniable advantage in term of power deposition with very low levels of $Q_{//}$ and the absence of ELMs.

An extrapolation based on these previous results, the limitation of critical flux on neutralisers and a significant part of radiated power (60 %) lets consider a maximum injectable power of 50 MW on Tore Supra. Moreover, the ergodic divertor which is an open divertor is characterized by a gradual detachment (plasma-neutral interaction is only bounded by the plasma) in comparison with the abrupt transitions to detachment in axisymmetric divertor experiments when critical neutral densities are achieved (mechanical baffling neutrals in divertor volume). The ergodic divertor offers a unique opportunity to operate an open divertor configuration with neutral baffling by the plasma itself [Ghe 99].

The multiplicity of the machines equipped with axisymmetric divertor, the vastness of the volume of experiments and results have certainly weighed in the decision of the choice for ITER. However the studies on ergodicity will continue on others tokamaks : a dynamic ergodic divertor (DED) is currently installed on TEXTOR.

7. Conclusion

An overview of the main results about power deposition experimental investigation with the ergodic divertor has been presented. Appropriate diagnosis measurements have led to a general survey which brings out several crucial point :

- Ergodic divertor has demonstrated a major advantage in term of power deposition (low heat flux...), large particle screening and high radiation capability compared to the limiter.
- With regard to the heat flux different conclusions should be pointed out : heat flux grows in a quasi linear way with the divertor current which

determines the amplitude of the perturbation; different behaviour as a function of $\langle n_e \rangle$ and impurity or additional power injection have been highlighted leading to the tendency : all that provides power shifts towards the high densities and all that consumes power (like radiation) shifts towards the low densities; deuterium and helium discharges show different levels of energy deposition; standardization of the power deposition at strong power level is observed.

- The standard value close to 7 is always recovered in ohmic discharges as expected in usual theory and simulations. However, it is worth noting that specific cases with low values exist, in particular for helium ohmic shots. For these latter shots, the electron temperature given by the Langmuir probes is overestimated with the probable presence of an energetic tail in the electronic distribution function. An increase of γ_{exp} is observed with the total input power independently of the working gas.
- The heat flux on the neutralizer plates shows a clear behaviour as the plasma detaches allowing to take into account the overall heated surface of the plate. The advantages of infrared thermography in term of spatial resolution has led to a layout of 2D DoD map with a possible space-time analysis. With its great flexibility, "IR" DoD emphasizes the double role of the thermal imaging diagnostic : measurements of the absolute surface temperature on the plasma facing components preventing a risk of overheating and now detachment characterization.
- Finally, from the obtained experimental results, extrapolations let foresee an operation up to 50 MW of injected power in Tore Supra. Such performance would provide the reason to carry on to evaluate the merits of

this configuration. A possible strategy to use ergodic divertor in future devices is considered. An optimised design and an operation with both large enough additional heating is necessary. This concept could be indeed very complementary to axisymmetric divertor. Perhaps that the ideal solution would be a ergodisation of the axisymmetric divertor...

Références

- [Azé 00a] Azéroual A., Pégourié B., Chareyre E. et al 2000 Nucl. Fusion **40** 1651
- [Bat 97] Batishchev O.V., Krasheninnikov S.I., Catto P. J. et al 1997 Phys. Plasmas **4** (5) 1673
- [Bir 91] Birdsall C. K. IEEE Transactions on Plasma Science **19**, 65 1991
- [Cos 01a] Costanzo L., Gunn J.P., Loarer T. et al, 2001 J. Nucl. Mater. **290-293** 840
- [Cos 01b] Costanzo L., Loarer T., Gauthier E. et al Proc. 28th EPS Conf. on Plasma Physics and Controlled Fusion 2001 Funchal, Portugal
- [DeM 95] DeMichelis C., Grosman A., Garbet X. et al 1995 Nucl. Fusion **35** 1133
- [Gau 01] Gauthier E. Private communication
- [Ghe 99] Ghendrih Ph., Grosman A., Gunn J.P. et al 1999 J. Nucl. Mater. **266-269** 189
- [Ghe 97] Ghendrih Ph. and Tore Supra team 1997 Plasma Phys. Control. Fusion **39** B207
- [Ghe 96] Ghendrih Ph., Grosman A., Capes H. 1996 Plasma Phys. Control. Fusion **38** 1653
- [Gro 01] Grosman A., Ané J.M., Barabaschi P. et al Proc. 28th EPS Conf. on Plasma Physics and Controlled Fusion 2001 Funchal, Portugal
- [Gro 97] Grosman A., Ghendrih Ph., Meslin B. et al 1997 J. Nucl. Mater. **241-243** 532
- [Gro 92] Grosman A., Ghendrih Ph., DeMichelis C. et al 1992 J. Nucl. Mater. **196-198** 59
- [Gun 99] Gunn J.P., Azéroual A., Bécoulet M. et al 1999 Plasma Phys. Control. Fusion **41** B243
- [Kra 95] Krasheninnikov S.I., Catto P.J., Helander P. et al 1995 Phys. Plasmas **2** (7) 2717
- [Mon 01] Monier-Garbet P., Clement C., Corre Y. et al Proc. 28th EPS Conf. on Plasma Physics and Controlled Fusion 2001 Funchal, Portugal
- [Pit 97] Pitcher C.S. and Stangeby P.C. 1997 Plasma Phys. Control. Fusion **39** 779
- [Tho 01] Thomas P. et al Proc. 28th EPS Conf. on Plasma Physics and Controlled Fusion 2001 Funchal, Portugal
- [Ver 93] Verboncoeur J.P., Alves M.V., Vahedi V. et al 1993 J. Comp. Phys. **104** 321
- [Ver 95] Verboncoeur J.P., Langdon A.B. and Gladd N.T., 1995 Comp. Phys. Comm. **87** 199

Code available via <http://ptsg.eecs.berkeley.edu/>

Figure captions

Figure 1 : Module of the ergodic divertor (six are equally spaced toroidally inside the vacuum vessel).

Figure 2 : Neutraliser plate equipped with Langmuir probes (three can be seen on the picture)

Figure 3 : Thermal view of the neutraliser plate (the same as figure 2). Hot spots correspond to Langmuir probes (except on the left side).

Figure 4 : Evolution of the parallel heat flux profile (along the neutraliser plate) as a function of the divertor current.

Figure 5 : Evolution of the parallel heat flux (deduced from infrared measurements) as a function of the conducted power.

Figure 6 : Evolution of the parallel heat flux (calculated with the Langmuir probes) with and without neon injection as a function of the volume averaged density.

Figure 7 : Parallel heat flux (at the neutralizer plate) as a function of the volume averaged density for different ICRH heating levels.

Figure 8 : Infrared mean parallel heat flux as a function of the total input power for helium discharges (circles) and deuterium discharges (triangles).

Figure 9 : Evolution of the parallel heat flux profile for different ICRH heating levels.

Figure 10 : Experimental sheath heat transmission factor as a function of the total input power for helium shots (circles) and deuterium shots (triangles).

Figure 11 : Experimental sheath heat transmission factor as a function of the edge temperature for an ohmic helium shot (cross) and an ohmic deuterium shot (circles).

Figure 12 : Evolution of the edge temperature deduced from Langmuir probes and infrared thermography as a function of the volume averaged density.

Figure 13 : Evolution of the parallel heat flux as a function of the edge temperature.

Figure 14 : Temporal evolutions of the probe DoD and the infrared DoD.

Figure 15 : Evolution of the infrared representation of the neutraliser plate at three characteristic times.

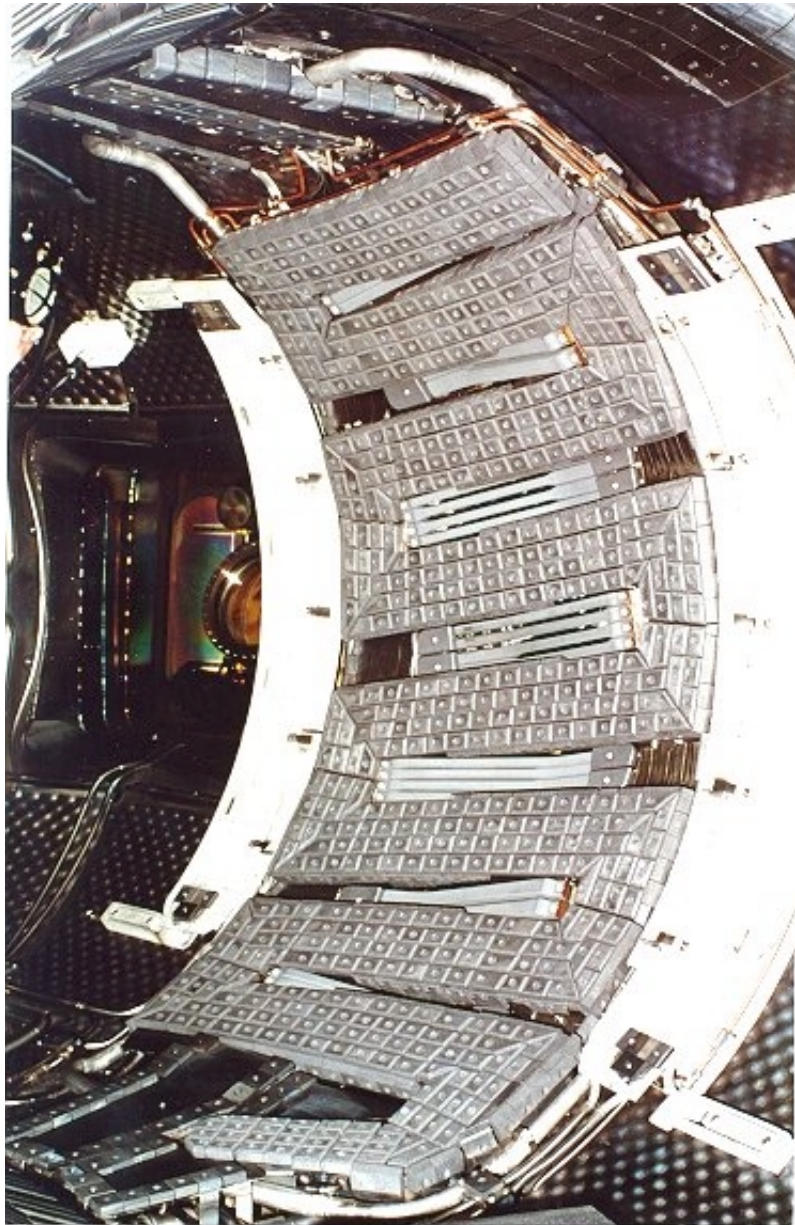


Figure 1



Figure 2

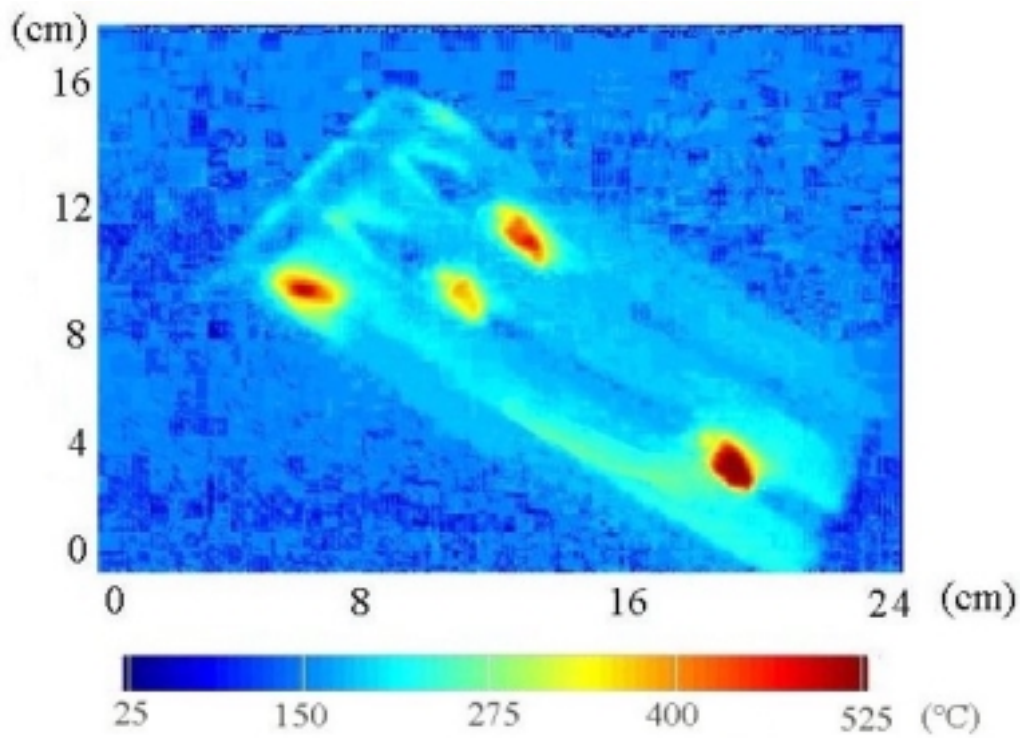


Figure 3

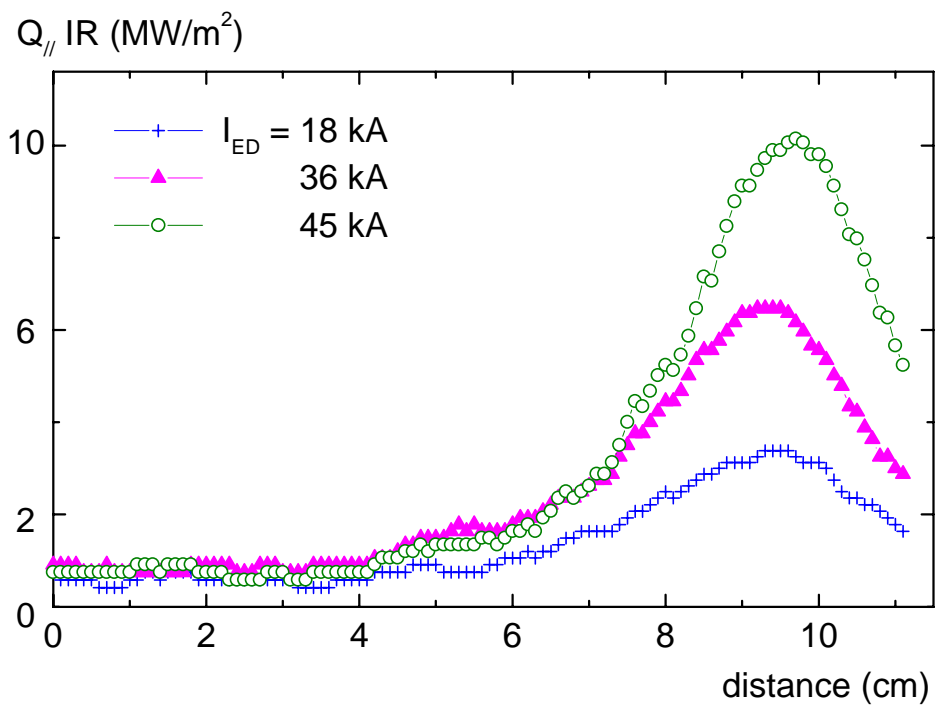


Figure 4

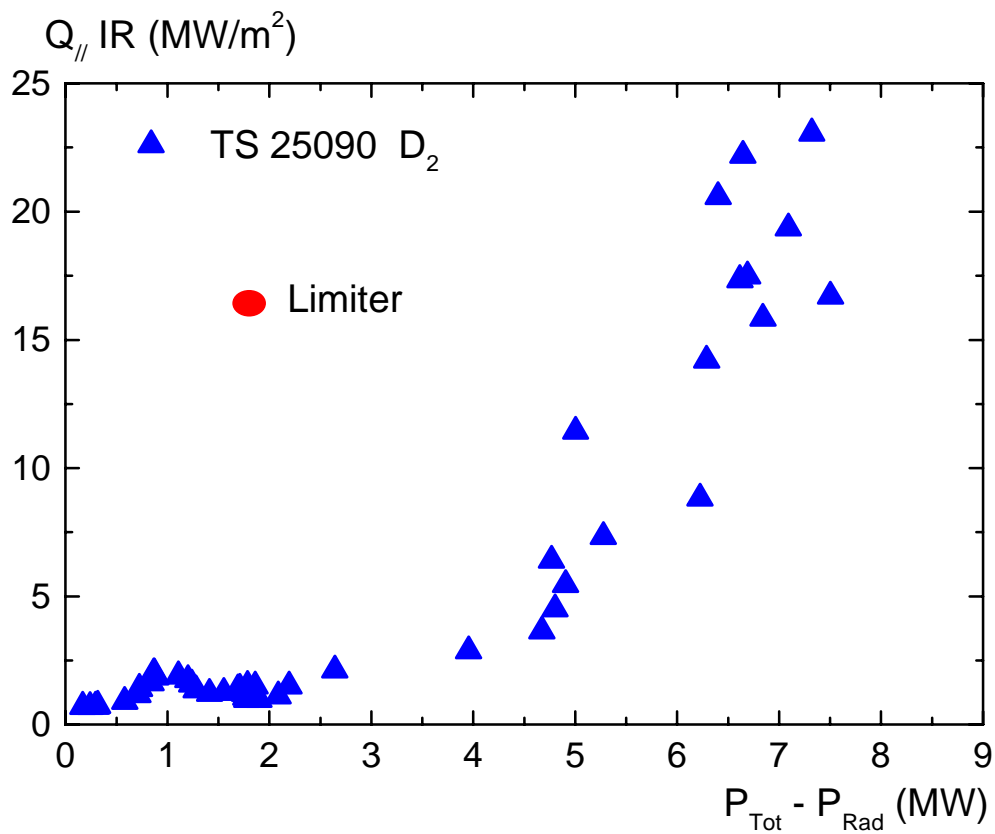


Figure 5

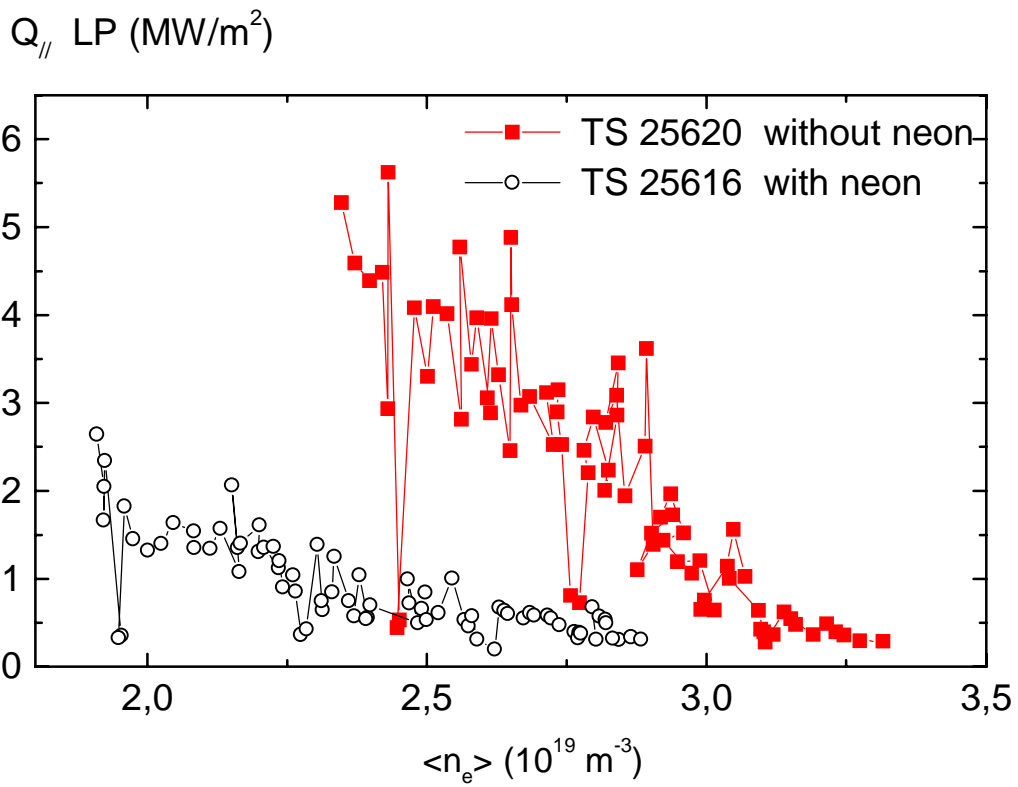


Figure 6

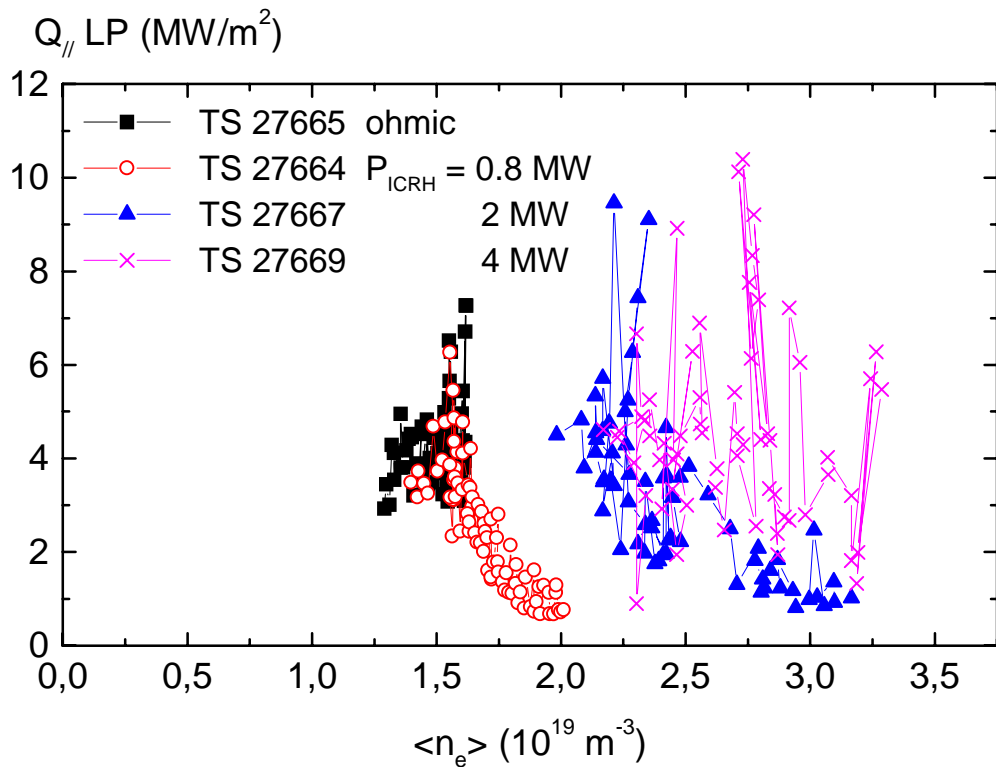


Figure 7

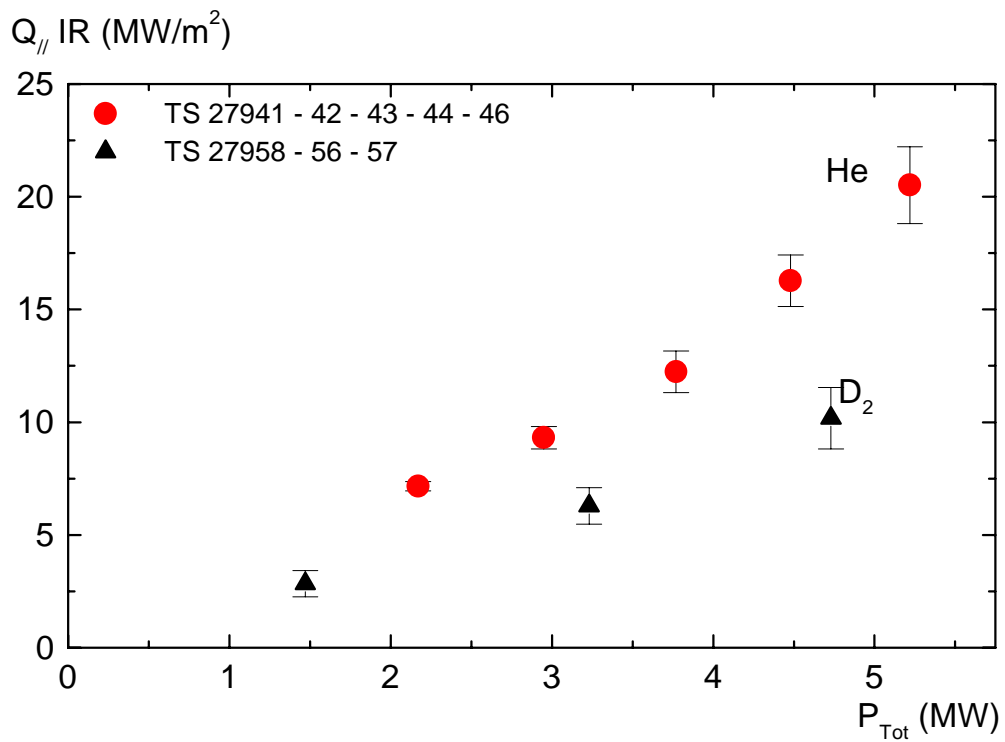


Figure 8

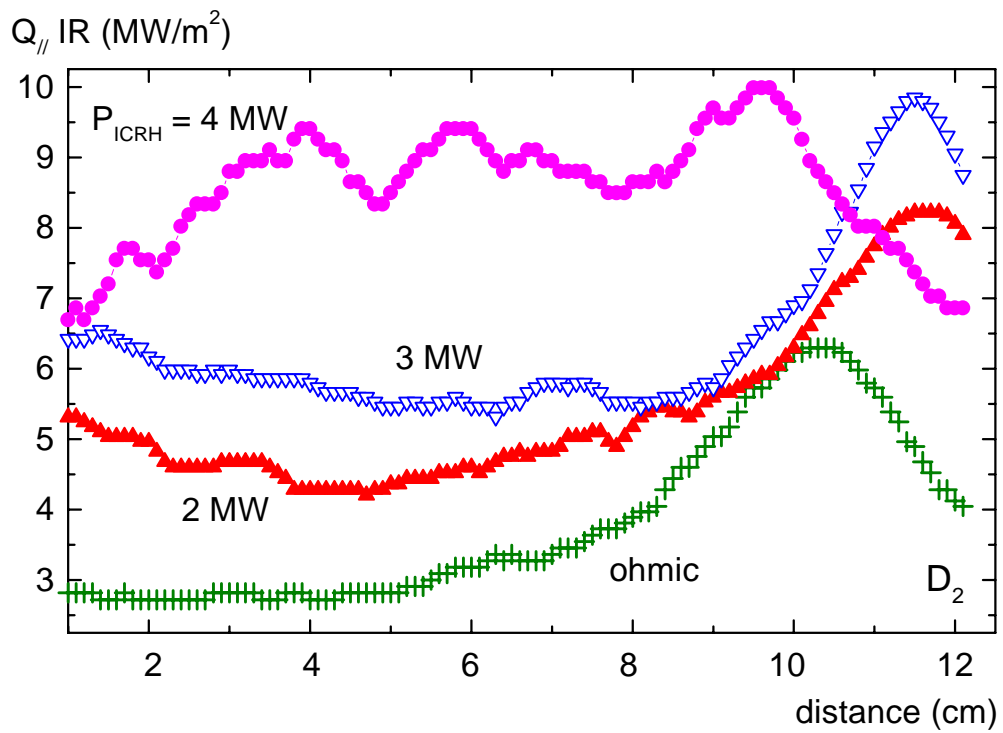


Figure 9

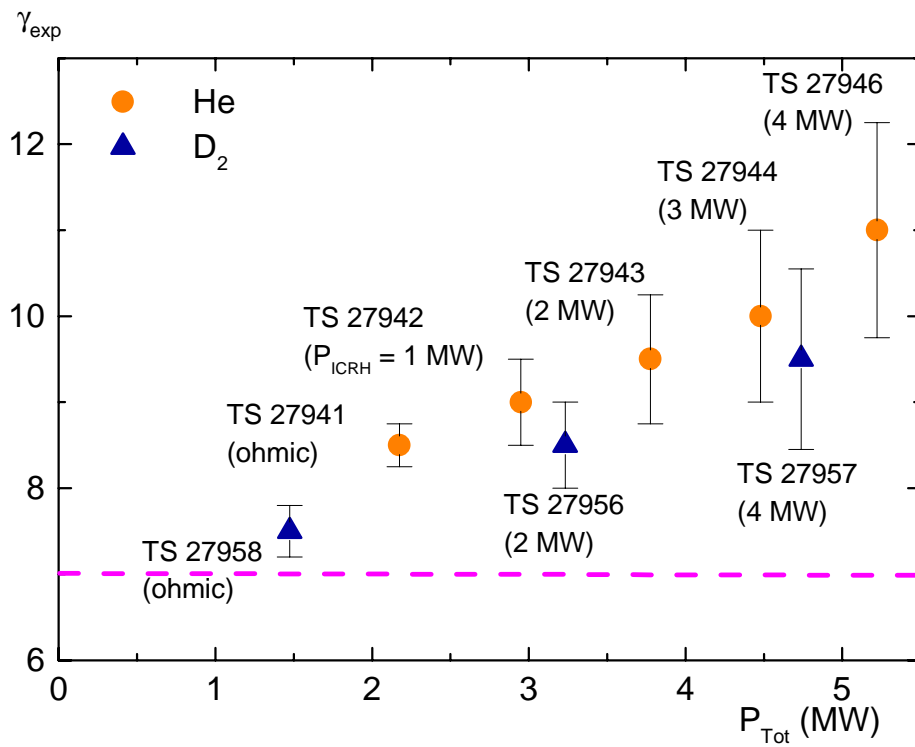


Figure 10

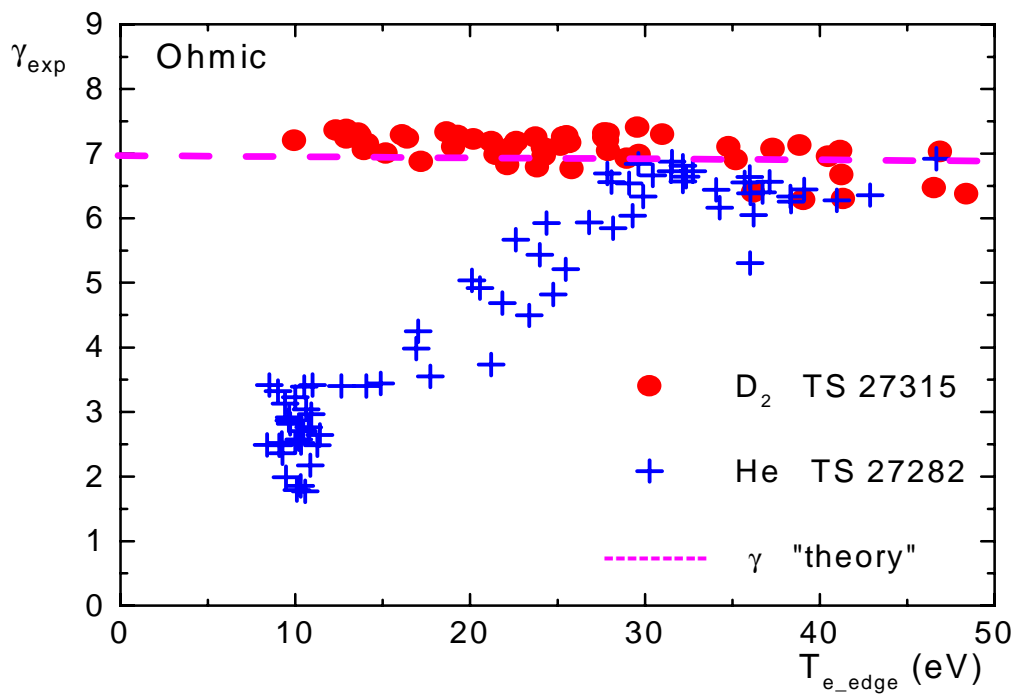


Figure 11

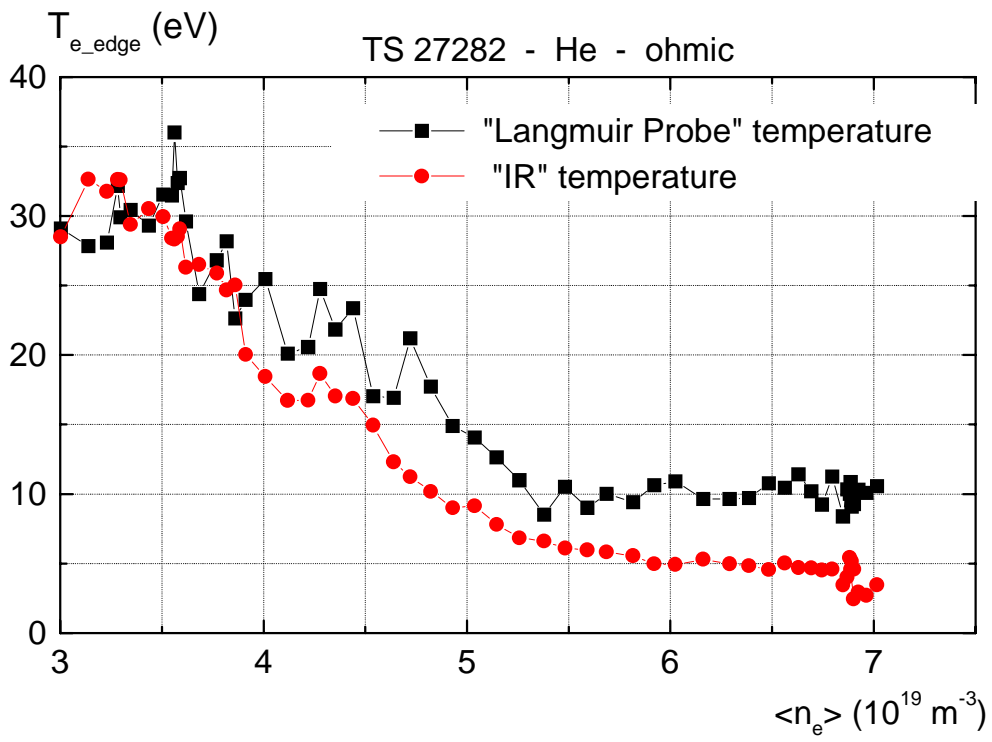


Figure 12

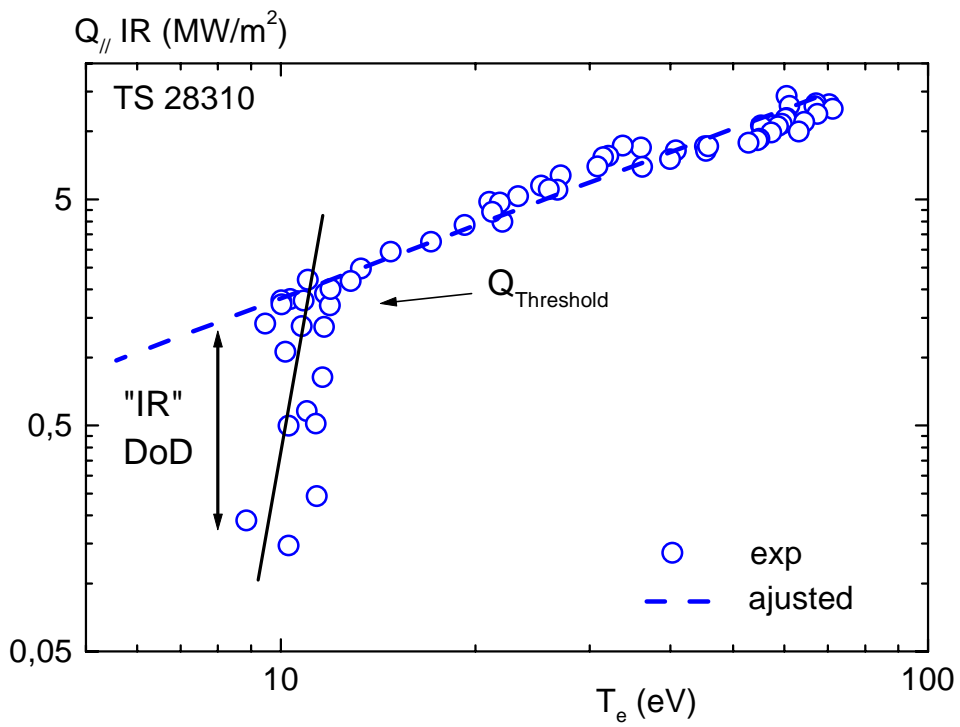


Figure 13

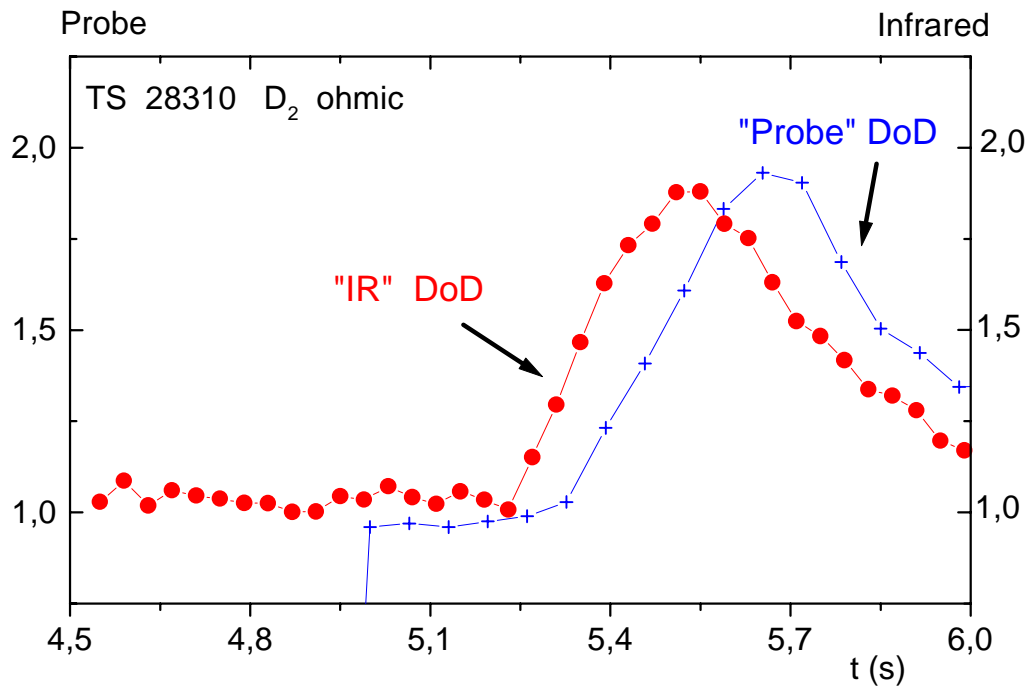
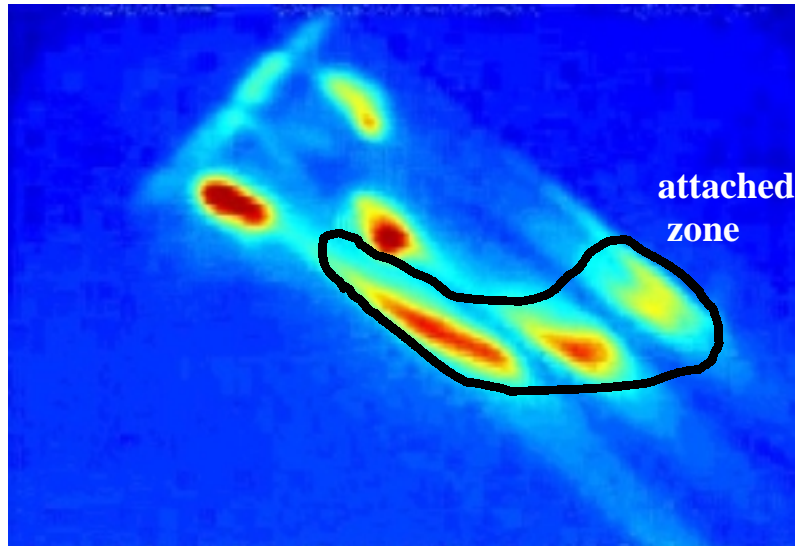


Figure 14

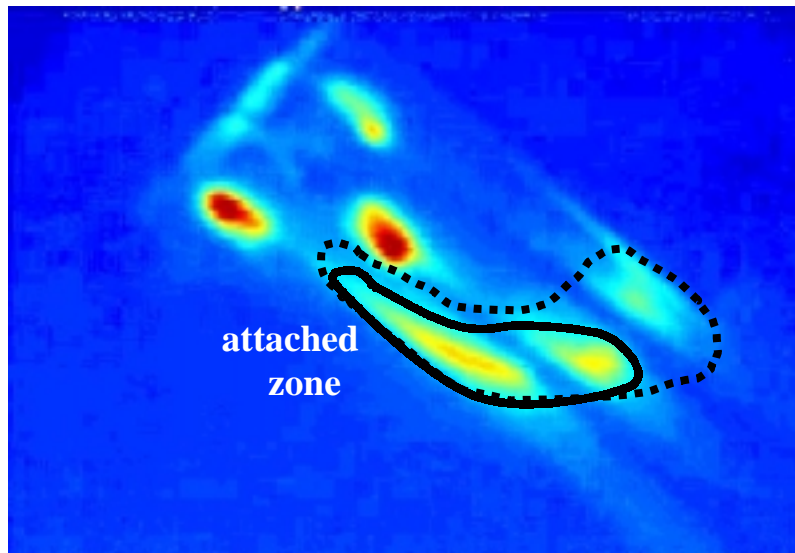
Attached

$t = 4 \text{ s}$



Semi-detached

$t = 5 \text{ s}$



Detached

$t = 5,25 \text{ s}$

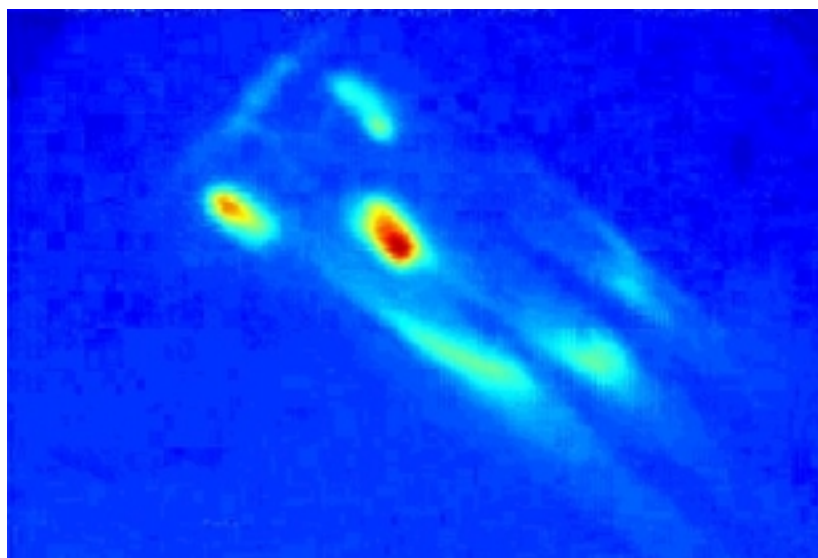


Figure 15